

See discussions, stats, and author profiles for this publication at: <https://www.researchgate.net/publication/236082364>

On the Nature of Hypercoordination in Dihalogenated Perhalocyclohexasilanes

ARTICLE *in* THE JOURNAL OF PHYSICAL CHEMISTRY A · MARCH 2013

Impact Factor: 2.69 · DOI: 10.1021/jp401210c · Source: PubMed

CITATIONS

9

READS

38

3 AUTHORS, INCLUDING:



Vijay Solomon

University of South Carolina

21 PUBLICATIONS 142 CITATIONS

[SEE PROFILE](#)

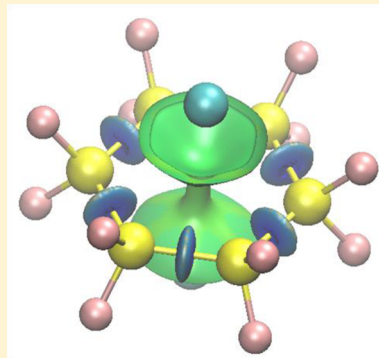
On the Nature of Hypercoordination in Dihalogenated Perhalocyclohexasilanes

Swaminathan Angeline Vedha, Rajadurai Vijay Solomon, and Ponnambalam Venuvanalingam*

Theoretical and Computational Chemistry Laboratory, School of Chemistry, Bharathidasan University, Tiruchirappalli 620024, Tamil Nadu, India

S Supporting Information

ABSTRACT: Hypercoordination in silicon has long been reviewed. Dihalogenated perhalocyclohexasilane inverse sandwich complexes (ISCs) are the only group of hypercoordinate Si complexes with anion donors that contact six neutral silicon atoms; opening prospective applications in Si self-assembled nanostructures. Hypercoordinate bonds in 16 such ISCs were studied and their anion ring interactions have been understood with respect to halides. μ^6 mode of coordination was confirmed by the presence of 6 equivalent (3,-1) bond critical points through Bader's QTAIM perspective. The presence of Lewis acid sites above and below the flat Si rings were examined through a reduced density gradient (RDG) analysis, and the ability of halide anions ($X' = F, Cl, Br, I$) to hypercoordinate has been understood. Role of the ring halides (X) in tuning size and acidity of Lewis sites has been addressed. While the total interaction between the two anions and the ring is quantified through EDA, each SiX' hypercoordinate bond was identified as either purely ionic or transient through QTAIM computations. CDA shows that these complexes are of donor–acceptor type with significant back-donation. The analysis shows that BrF^- and IF^- were found to reach maximum covalency within the group. Hence in future, tuning these ISCs for construction of nanocrystalline Si structures for optoelectronic properties can essentially utilize the collective, weak yet hypercoordinate Si in these complexes.



1. INTRODUCTION

Silicon, the metalloid that makes the integrated chips (ICs) of present day gadgets, the second most abundant in earth's crust and an essential element in biology, is less reactive than its chemical analogue carbon, but it has displayed a kaleidoscope of compounds with its ability to extend its valence.^{1–9} Though tetrahedron is the common geometry of Si in nature, quite a few nontetrahedral Si complexes have also been synthesized so far. Those with higher than tetrahedral coordination are termed hypercoordinate by Schleyer.¹⁰ Recently, pentacoordinated Si in silacyclophanes have been investigated theoretically by Doronina et al.¹ Hexacoordinate aromaticity in phthalocyanins have been reported by Yango in an effort to reduce the disaggregation of the carbon analogues of phthalocyanins.¹¹ Octahedral $HSiCl_2$ Me adducts with pyridine have been reported by Fester et al.¹² where the two nitrogens of pyridine hypercoordinate to Si. A few hepta coordinate halosilanes were also synthesized by Kobayashi et al. and were found to be good candidates for nucleophilic substitution.¹³ These hypercoordinate Si compounds have interesting properties like aromaticity,¹⁴ fluxtionality,⁴ and diverse reactivity¹⁵ as well as prospective applications in optoelectronic devices,¹⁶ semiconductors, and in Si-based laser technology.¹⁷

Interestingly, of all these hypervalent Si complexes, the only known examples with donor ligands contacting more than three Si atoms are the dianion and pseudo halide coordinated perhalocyclosilanes, reported by Dai et al.^{18,19} The hyper-

valency exhibited by more than one Si atom in a plane in this inverse sandwich complexes (ISC), opens up their utility in forming stacked structures and as building blocks for nanosystems and hence are investigated in the present work (Figure 1). It is well-known that the quantum confinement and nontoxicity makes Si nanocrystals attractive candidates in nanoscience and technology. Recently, Vach has designed a novel nanocrystal of Si, which is aromatic and electron deficient due to Si hypercoordination.^{20,21} In pursuit of building blocks to create new silicon landscapes, Zdetsis² have done a DFT study of multidecker SiC sandwiches and has shown that the interstitial metals play a vital role in the stability and the magnetic property of such multidecks.

We present the DFT study of these perhalogenated cyclohexasilane inverse sandwich complexes for their potential in forming stacked structures where the halide ions in-between can have useful electron transport properties. Complexes studied herein, synthesized by Boudjouk et al.,²² were found to exhibit inverse sandwich structures in the solid state where the six Si atoms form a planar hexagon with two halide anions occupying the positions one above and the other below the ring (Figure 1). The $Si_6X_{14}^{2-}$ dianions exhibit novel μ^6 coordination, where each apical halide coordinates to six Si atoms in a ring

Received: February 2, 2013

Revised: March 26, 2013

Published: March 26, 2013

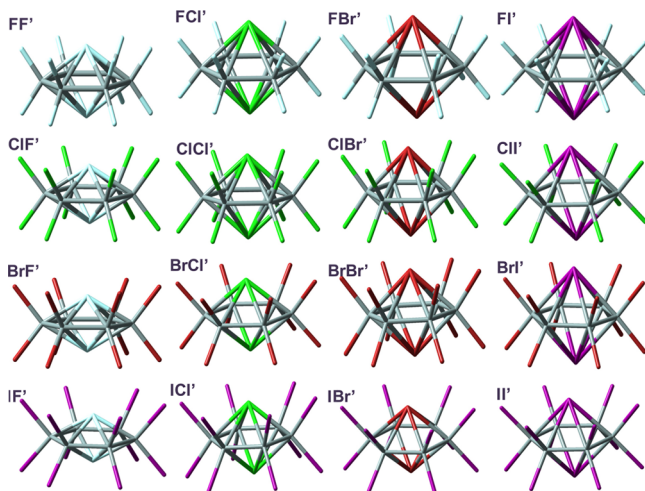


Figure 1. B3LYP/6-311++g(d,p) optimized geometry of ClI' chosen for the study.

and every Si is in a distorted octahedral geometry.²³ The reason for the planarity of the ring has been attributed to the suppression of pseudo Jahn–Teller effect (PJT) by the donation of a pair of electrons to the ring, reducing the HOMO–LUMO gap and hence lifting the degeneracy, but the nature of the anion binding and the Si-extra coordinate bonds has not been addressed so far.

Hence, an attempt has been made to understand hypercoordination expressed in terms of the extent of covalency of the anion-ring interaction by the partitioning scheme and to identify the nature of the μ^6 mode of coordination through the electron density distribution in the atomic basins of the hypercoordinating atom through a QTAIM perspective.²⁴ The corresponding natural bond orbitals are examined to correlate with the Lewis structures. Sixteen ISCs each with a planar Si₆ ring core, 12 ring halides (X), and 2 apical halide ions (X') are chosen for the study and are labeled as XX' throughout the discussion.

2. COMPUTATIONAL DETAILS

Crystallographic data of the geometries of the inverse sandwich complexes (ISCs), with X = Cl, Br, I and X' = Cl and Br, were retrieved from that reported by Boudjouk et al.²³ Earlier reports suggest that B3LYP functional performs well in predicting bonding situation in perhalosilane systems,^{9,25} other silicon hypercoordinated compounds,^{26–29} and in silicon clusters.^{7,30,31} Hence, the same was adopted here. Sixteen titled cases of which one is represented in Figure 1 were optimized with D_{6h} symmetry at the B3LYP³²/6-311++g(d,p) level with pseudo potentials on the iodine atoms at the SDD³³ basis set using the G09W³⁴ suite of programs. NBO analysis was carried out using G09W at the same level.³⁵ The calculated bond parameters correlate well with the experiments (Table 1). Zeigler's energy decomposition analysis (EDA) was performed at GGA/BP86³⁶/DZVP with ZORA using ADF2008.³⁷ The instantaneous interaction energy between the two fragments has been calculated using the following equation:

$$\Delta E_{\text{int}}(\zeta) = \Delta E_{\text{elstat}}(\zeta) + \Delta E_{\text{pauli}}(\zeta) + \Delta E_{\text{orb}}(\zeta) \quad (1)$$

and the percentage covalency of the hypercoordinate bonds have been calculated using eq 2

Table 1. Calculated Bond Parameters of Optimized Geometries at B3LYP/6-311++g(d,p); Bond Lengths in Å Units

ISC	N _(IMG) ^a	Si–Si	Si–X'	Si–X	X–X'	X'–Si–X
		(Å)				(Å)
FF'	5	2.313	2.697	1.661	3.380	98.926
FCl'	0	2.356	3.113	1.654	3.509	89.379
FBr'	0	2.362	3.144	1.656	3.527	89.000
FI'	-1	2.410	3.532	1.709	3.761	69.086
CIF'	5	2.327	2.689	2.131	3.684	99.050
ClCl'	0	2.372	3.085	2.123	3.729	89.500
		2.36 ^b	3.06 ^b	2.11 ^b	3.90 ^b	
ClBr'	0	2.379	3.123	2.129	3.755	89.200
ClI'	0	2.398	3.473	2.122	3.863	83.590
		2.337 ^b	3.271 ^b	2.088 ^b	3.709 ^b	
BrF'	3	2.315	2.669	2.286	3.756	98.300
BrCl'	0	2.359	3.066	2.284	3.774	88.450
BrBr'	0	2.368	3.090	2.290	3.805	88.660
		2.350 ^b	3.061 ^b	2.229 ^b		
BrI'	0	2.451	3.500	2.396	4.068	85.080
		2.356 ^b	3.238 ^b	2.293 ^b	3.892 ^b	
IF'	9	2.364	2.695	2.568	4.068	101.210
ICl'	3	2.458	3.135	2.689	4.042	87.570
IBr'	0	2.428	3.192	2.568	4.087	89.700
II'	0	2.447	3.429	2.571	4.147	86.200

^aNumber of imaginary frequencies. ^bAveraged experimental parameters as reported in the references.

$$[\Delta E_{\text{orb}}(\zeta) / (\Delta E_{\text{elstat}}(\zeta) + \Delta E_{\text{orb}}(\zeta))] \times 100 \quad (2)$$

The nature of the charge decomposition in the ISCs was analyzed using the charge decomposition analysis (CDA) partitioning scheme³⁸ as implemented in QMforge. Since earlier efforts to understand the hypo- and hypervalent bonds within the “Atoms in Molecules” formalism have proved very successful,^{39–43} we adopt the same for these ISCs also. Bader's analysis is carried out in both Multiwf⁴⁴ and AIM2000⁴⁵ using extended wave function files generated at the B3LYP/6-311G+(d,p) level with SDD-based pseudo potentials on the iodine atoms and wave function files at all-electron basis computed at the B3LYP/6-311G++(d,p), respectively.

3. RESULTS AND DISCUSSION

3.1. Optimized Geometries and Their Stabilities. Bond parameters of complexes of Si₆X₁₂X'₂²⁻ where X = X' = F, Cl, Br, and I optimized with D_{6h} symmetry are listed in Table 1. Frequency calculations were carried out on the optimized geometries, and results reveal that all structures correspond to minima except structures FF', FI', CIF', BrF', IF', and ICl', which were higher order saddle points and efforts to reoptimize them also resulted in the same structure in line with the earlier report.²⁵ Ground state geometries of these structures were found to be of D_{3h}, D₃, C₂, and C_s symmetries.

Si–X' bond lengths in all the ISCs studied here were found to be considerably shorter than the sum of their van der Waals radii but longer than their covalent radii. For instance, the Si–I bond lengths are expected to have a van der Waals radii of 4.08 Å⁴⁶ and a covalent radii of 2.50 Å,⁴⁷ while it ranges from 3.43 to 3.53 Å in ISCs with X' = I. In ISCs with X' = Br, Si–X' bond lengths are 3.09 to 3.14 Å, while the expected van der Waals radii and covalent radii were 3.95 and 2.31 Å, respectively (Table 1). This indicates the existence of bonding interactions. The bond angle around the Si atom is consistent with that of a

distorted octahedral. As the size of the apical halide increases, the less close it is to the center of mass of the ring halides (Supporting Information, Table S1). In all the ISCs with F^- as apical halides, the apical halides were present well below the center of mass of the ring halides, and in FF' , it is much closer, indicating that the fluorides being smaller than the other halides were entrapped into the ring easily. When the iodides are the apical halides, they lie well above the ring center created by the six ring halides. Bromides and chlorides are just above the center of the ring. Hence, it is obvious that the size of the apical halides dictates their entrance to the Si_6 ring core. The distance between the apical and the ring halide are longer than the sum of their van der Waals distances (Table 1). Therefore, it is true that the ring and apical halides are not involved in any favorable halide interactions as reported earlier.⁴⁸

A glance at the van der Waals surfaces of the ISCs (Supporting Information, Figure S1) shows the space available for the various apical halides and how they can be accommodated. In the case of FI' , the apical halides are protruding out of the ring, and in IF' , the apical halides are deeply buried. $BrBr'$, $BrCl'$, $ClCl'$, and $ClBr'$ form a subclass where the apical halides fit in the cavity of the ring. Hence, from the geometric parameters, it is evident that the position of the apical halides depends on the size of the ring halides, while they do not interact with the ring halides.

3.2. Energy Decomposition Analysis (EDA). According to the Lewis Langmuir Octet rule, a contribution of less than 33% ionicity by constituent atoms would lead to hypervalent bonds in trivalent compounds.⁴⁹ Hence, in an effort to understand the dianion to Si ring interaction, the percentage covalency between apical halides and the Si_6 core is computed by partitioning the apical halides and the perhalosilane rings as part of two fragments, through energy decomposition analysis based on Ziegler's scheme,³⁷ and the results are represented in Figure 2.

The order of increasing covalency of the ring to apical halides is as follows: $FI' < FBr' \approx FCl' < ClI' < ClF' < BrI' \approx ClBr' < FF' < ClCl' < II' < BrBr' < BrCl' \approx IBr' < ICl' < BrF' < IF'$. Complexes with less than 44% of covalency are classified as Type-1, and those with covalency ranging from 48 to 58% are

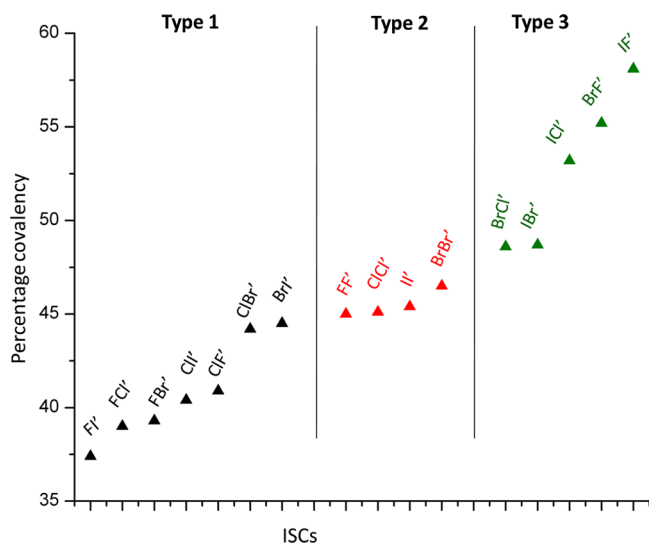


Figure 2. Classification of ISCs based on percentage covalency computed from EDA at BP86/DZVP level.

termed as Type-3 complexes. Within the range of 45 to 47% lie all ISCs of the $X = X'$ kind, and they are grouped as type-2 ISCs (Figure 2).

3.3. Reduced Density Gradient Analysis (RDG). It has already been proposed that the region that lies along the centriod running through the six-membered ring possess sites of depleted electron density called Lewis acid sites, on which the apical halides are accommodated.⁴⁸ The nature and acidity of these sites seems to play a directive role in the halide coordination. A RDG method based analysis has been performed to identify these sites. Recently, an index for identifying and analyzing the noncovalent interactions (NCI) based on the electron density and its reduced gradients has been introduced by Yang et al.⁵⁰ In NCI indexing, all of the interactions with at least a specified fraction of the density from within a molecule are turned off, screening out only the intermolecular interactions.

The NCI plot depicts the strength of interactions through color codes: red signifies strong repulsion, green stands for weak interactions, and blue signifies strong attractions. Three dimensional NCI plots of XX' complexes are shown in Figure

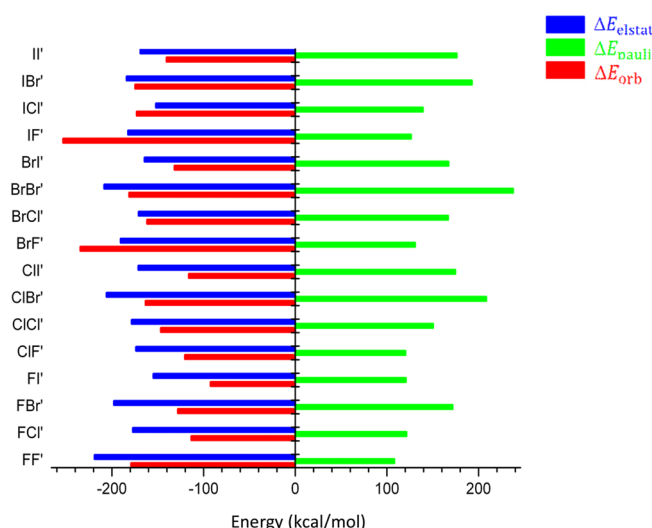


Figure 3. EDA results for $[Si_6X_{12}X'_2]^{2-}$; $X/X' = F, Cl, Br$, and I .

4, where surfaces correspond to an isovalue of 0.3 a.u. and a color scale of $-0.1 < \rho < 0.1$ a.u. From the figure, it is clear that all the complexes have acidic sites that are seen as a green/greenish blue region running through the centriod of the Si_6 ring. The color of the acidic site tells about the nature of the interactions by which it holds the apical ion. It is interesting to see the small size F^- ions strongly bound (greenish blue color) inside the cavity compared to largely polarized I^- ions (green color). This shows the weakly bound nature of I^- ions in the acidic pocket. It is noteworthy to see that, as the size of the apical ion increases, the ability to bind in the acidic pocket decreases. For instance, the F^- ions are very close to the acidic pocket, whereas I^- ions are pushed away from the acidic pocket. On moving from FF' to II' , the strong attractive interactions (blue color) slowly turned into weak interactions (green color). This is well corroborated with the EDA and ELF analysis.

Two-dimensional ELF⁵¹ (electron localization function) filled color diagrams of the 16 ISCs were constructed on the plane just below the apical halides, where the Lewis acid sites are present (Supporting Information, Figure S2). The color

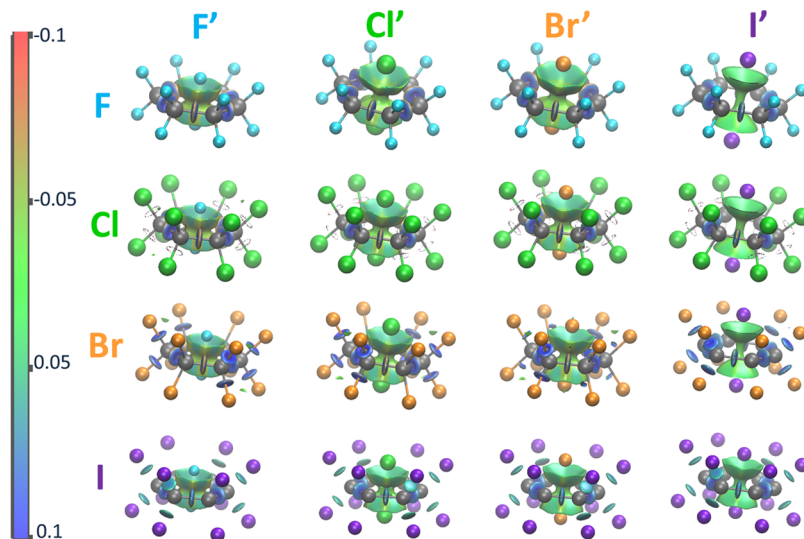


Figure 4. Three-dimensional NCI plot of the ISCs where isosurfaces correspond to an s value of 0.3 a.u. and the RGB scale ranges from $-0.1 < \rho < 0.1$ a.u.

code is defined in the bar displayed along the figure. Lewis acid sites are seen as regions of pale blue color at the center of the ring where the $\eta(r)$ value is approximately 0.05.^{52,53} These sites are also vividly revealed in the NCI 3D plots⁵⁰ where the green region represents a strong attractive interaction (Figure 3).

From Figure 2, it is clear that IF' has the greatest percent covalency of interaction among all the ISCs. This is due to the ease in confining the small and weakly polarizable F⁻ ion on the small and weak Lewis acid sites created by the less electronegative iodides above and below the ring. In all the ISCs with weak acid sites holding small or reasonably sized X's that are either poorly or moderately polarizable have higher percentage covalency of interactions and therefore are conveniently placed to hypercoordinate with Si and share electron density with ease. Such systems with X = I and Br and X' = F, Cl, and Br are classified as type-3 hypercoordinating complexes.

On the other end of the series (type-1, Figure 2), coordination of highly polarizable I⁻ ion on the strong acidic site created by the fluoride ring halides seems to have poor covalency due to the volume of the apical ion. (The diameter of the cavity is found to be 7.06 Å, while the volume of I⁻ is 25.72 cm³/mol.) Moreover, the apical iodides are placed far away from the center of mass of the ring (i.e., 2.58 Å), preventing them from satisfying the Lewis acid sites. This effect is also seen in all ISCs with either X = F and Cl or X' = I and Br'.

One anomaly in Type-1 is ClF', which is expected to be among the ISCs of type-3. Its present position is attributed to the lesser contribution from stabilizing interactions. Among the type-2 systems, where X = X' (the effects due to cavity sizes are concealed), BrBr' is found to have higher covalency. While FF' and ClCl' interactions are found to be more electrostatic, II' shows an increase in Pauli's repulsion. In summary, from EDA, it is possible to classify the coordinating ability in the ISCs into the above three types. ISCs IF', BrF', ClI', IBr', and BrCl' are found to experience higher covalency in the interaction than the other ISCs. The dianion ring interactions are decided primarily by the acidity and size of the Lewis acid sites and the polarizability of the anion. By depleting the electron density at the Si atom, the ring halides play the directive role in the anion ring binding mechanism. It is unfortunate that an ideal case of a

strong Lewis acid site entrapping a large polarizable donor ion is practically more ionic in its association with the Si₆ core.

In order to understand the fragment orbitals that contribute to the orbital interactions of the ISCs, segmented fragment orbitals (SFOs) are analyzed (Supporting Information, Table S2). SFOs are linear combinations of the valence fragment orbitals that transforms to the irreducible representations of the molecular symmetry group. Each SFO is characterized by an irreducible representation of the molecule that generates the fragment orbitals. The SFO analysis shows that the HOMOs and LUMOs are mainly the combinations of SFOs of ring fragments. Only in ISCs with X' = I and in ClBr' and BrBr' are the HOMOs majorly contributed by the SFOs of apical ions of π_{ux} and π_{uy} symmetry. In general, the interactions between the two fragments are mainly from the contributions of orbitals with π_u symmetries of apical ions and of B_{1u} and A_{1u} symmetries of the ring atoms.

3.4. Charge Decomposition Analysis. CDA allows the relative amount of electron donation (d), back-donation (b), and the interaction between the occupied orbitals of both fragments leading to repulsive polarization (r) to be calculated. CDA results are given in Table 2.

Results show that high donation and back-donation, negative polarization, and near zero residual charge indicate that these complexes are of donor–acceptor type.⁵⁴ The donation/back-donation ratio (d/b) shows there is a significant back-donation from the Si₆ core. The residual term Δ obtained by analyzing the unoccupied orbitals of both fragments is virtually zero meaning predominant donor–acceptor nature of ISCs. Molecular orbitals 27 and 68 of FCl', contributing most to the donation term and back-donation according to CDA, are depicted in Figure 5.

3.5. QTAIM Study. QTAIM describes the atoms inside a molecule as a region of space surrounded by surfaces of zero flux, where the Ehrenfest force acting over the basin of atoms will be equal and opposite to the forces acting on the interatomic surface. Such partitioning into subsystems helps to understand the bonding in hypercoordinating systems from a non-MO perspective.⁵⁵ Much earlier, Sidorkin et al. have designed neutral intramolecular complexes containing Si atoms anchored by two oxygens and have investigated the effect of

Table 2. Results of the Charge Decomposition Analysis (CDA) on the Set of Complexes Studied; $X' \rightarrow Si_6X_{12}$ Donation d , $Si_6X_{12} \rightarrow X'$ Back Donation b , $Si_6X_{12} \leftrightarrow X'$ Repulsive Polarization r

	CDA			
	d	b	r	d/b
FF'	-0.148	1.450	-0.989	0.102
FCI'	-0.148	1.820	-1.543	0.081
FBr'	-0.176	2.039	-2.612	0.086
FI'	-0.105	2.000	-1.841	0.053
ClF'	-0.141	1.768	-1.035	0.08
ClCl'	-0.151	2.332	-1.792	0.065
ClBr'	-0.163	2.677	-2.927	0.061
ClI'	-0.101	2.529	-2.482	0.04
BrF'	-0.196	1.646	-1.113	0.119
BrCl'	-0.208	2.179	-2.082	0.095
BrBr'	-0.247	2.480	-3.491	0.1
BrI'	-0.156	2.363	-2.536	0.066
IF'	-0.213	1.744	-1.108	0.122
ICl'	-0.214	2.278	-1.827	0.094
IBr'	-0.237	2.580	-2.859	0.092
II'	-0.428	2.994	-5.354	0.143

substituents on the silicon–oxygen hypercoordination.²⁹ They have classified ionic and weakly covalent cases of such complexes based on electron energy density at the bond critical points (BCPs).²⁹ In the present system of study, the nonequilibrium geometries are also included for the analysis as Pendas et al.⁵⁶ have established that the forces exerted on such systems are described well through the wave functions within the QTAIM formalism. Earlier studies^{57,58} have also shown that such systems can be investigated through QTAIM.

QTAIM computations were performed on the 16 ISCs under study, and the molecular graph of one representative case (ClCl') with characteristic critical points is represented in Figure 6. All the complexes studied were found to obey the Poincaré–Hopf relationship, i.e.,

$$n - b + r - c = 1 \quad (5)$$

where n , b , r , and c are the number of critical points of the order and rank, (3,-3), (3,-1),(3,+1), and (3,3), respectively.

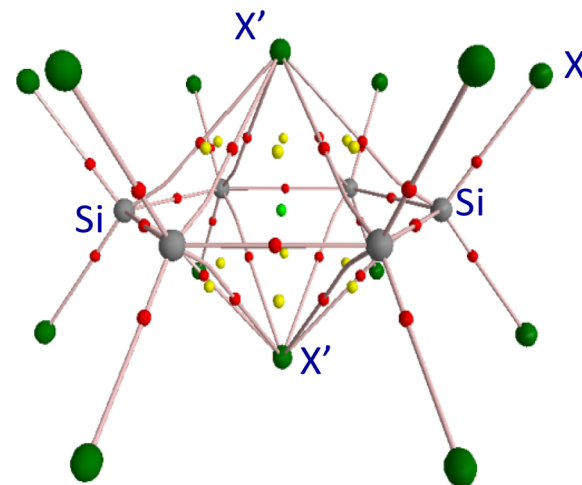


Figure 6. Molecular graph of ClCl' showing bond paths between Si and X'. BCPs are represented as small red spheres.

Molecular graphs of the 16 ISCs show similarity in pattern with 30 (3,-1) critical points, 12 (3,1) ring critical points formed at the 12 faces of the Si–X'–Si, and one cage critical point indicating the presence of preferred interaction between each apical halide and all the six Si atoms, indicating a μ^6 mode of bonding. Electron density at the BCPs between each Si and X' in all ISCs is invariably uniform. For instance, the $\rho(r)$ values at the BCPs between all the six Si and X' atoms in FF' is found to be 0.0207 a.u. Electron density at these critical points lie over the range of 0.020–0.013 a.u., which is much lower than the $\rho(r)$ at the Si–X bonds (of purely covalent nature) in these complexes (0.1 to 0.067 a.u.), and much lower than the $\rho(r)$ at the BCPs between Si–X of a pure coordinate bond of 0.078 a.u.¹¹ Therefore, the hypercoordinate bonds in the ISCs are ~ 4 and ~ 5 times weaker than the pure coordinate bonds and pure covalent bonds, respectively.

In ISCs with $X' = F$, BCPs lie much closer to the Si atoms, with positive Laplacian values at the BCP. This is because a basin of the more electronegative F⁻ overwhelms that of the Si and also because of the difference in their atomic radii. Figure 7a shows the gradient paths originating from the apical F and ring Br overwhelming the basin of the Si atom. The $G(r)/\rho(r)$ value, which scales the polarity of the Si–X' bonds, also reveals

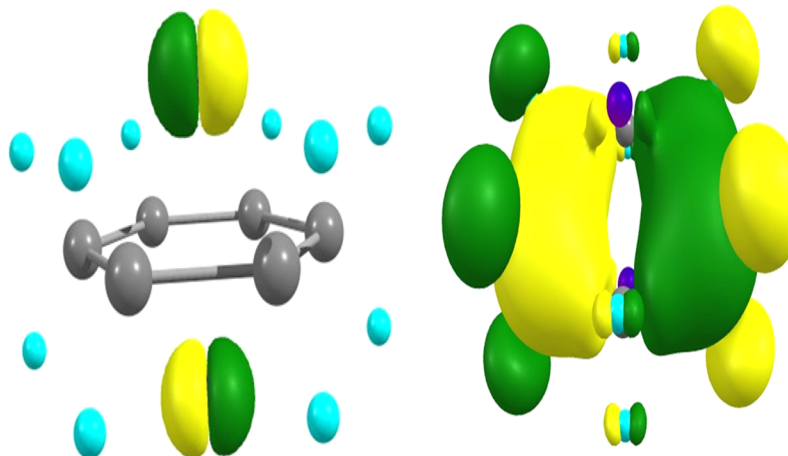


Figure 5. Donation (left) and back-donation (right) orbitals for FCl'.

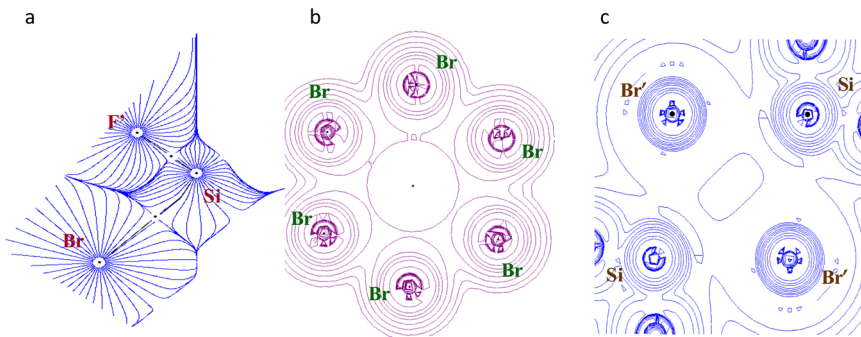


Figure 7. (a) Gradient vectors of the ring and apical halides in BrF'. (b) Contour plot of the Laplacian of rho cutting the plane containing the ring halides (Br') just below the apical (F'). (c) Contour map of electron density at the Si₆ core showing the VSCC and diffused valence shell of Br'.

Table 3. Topological Properties at One of the Si–X' BCPs Where $\rho(r)$ Values Are Reported in e/Å³ and $\nabla^2\rho$ Values Are in e/Å⁵

ISC	$\rho(r)$	Lapl	$H(r) \times 10^{-3}$	$G(r)/\rho(r)$	$K(r) \times 10^{-4}$	$ V(r) /G(r)$
FF'	0.021	0.05	-0.13	0.68193	0.13	1.02364
FCI'	0.017	0.04	0.37	0.54915	-0.37	0.99767
FBr'	0.019	0.04	-0.21	0.51405	0.21	1.00893
FI'	0.013	0.02	0.14	0.42317	-0.14	0.90598
ClF'	0.021	0.06	-0.001	0.67416	0.001	1.07024
ClCl'	0.018	0.04	0.12	0.54498	-0.12	0.98600
ClBr'	0.020	0.04	-0.43	0.5091	0.43	1.07746
ClI'	0.015	0.03	-0.01	0.43944	0.01	0.92095
BrF'	0.021	0.05	-1.21	0.66807	1.21	1.10977
BrCl'	0.019	0.04	0.09	0.54733	-0.09	0.98717
BrBr'	0.021	0.04	-0.65	0.51001	0.65	1.05920
BrI'	0.014	0.03	0.12	0.4275	-0.12	0.97939
IF'	0.021	0.05	-1.19	0.65799	1.19	1.07874
ICl'	0.017	0.04	0.27	0.51984	-0.27	0.95752
IBr'	0.019	0.04	-0.14	0.49185	0.14	1.02869
II'	0.016	0.03	-0.67	0.4392	0.67	0.98876

greater polarity of the Si–F' bonds. In the ISCs with X = X' = F, the ratio is at least thrice that of the ratio at the Si–I' BCP in X = X' = I.

The topological properties of the BCPs between the apical atoms (X') and Si are represented in Table 3. The magnitude of the properties at the (3,−1) BCPs between Si and X' follows the order, F > Cl ≈ Br ≫ I. From Table 3, it is evident that there is a uniform drop in the BCP properties as one goes from X' = F to I within each group. The positive Laplacian values at these BCPs for all ISCs indicate that the interacting basins are drawn toward the electropositive (Si) atoms as in any heteropolar bonds. The path lengths between Si and X' are not bifurcated equally by the BCPs, while the basins of the apical halides dominate the Si basins revealing a donor–acceptor relationship between the two. This is also inferred from the presence of zero-flux surfaces (or interatomic surface (IAS)) slightly closer to the Si atom and positive Laplacian values at the BCPs (Figure 7a). Hence, the Si–X' bonds are polar bonds in general.

Since QTAIM characteristics are typical of Si–X bonds, irrespective of the coordination number of Si, a comparison is drawn with other hypercoordinate Si bonds known earlier in the literature.^{29,59} Topological parameters of hypercoordinate Si complexes reported by Fester et al.,¹² Sidorkin et al.,²⁹ and Kocher et al.,⁶⁰ along with those of the present study, are listed in Table 4. From the Table 4, it is clear that halide coordination in ISCs of this study is much weaker than hypercoordinate complexes of Si known in the literature. The sign of $H(r)$

Table 4. Calculated ρ and $\nabla^2\rho$ Values of ClCl' and FF' from QTAIM in Comparison with Literature Where $\rho(r)$ Values Are in e/Å³ and $\nabla^2\rho$ Values Are in e/Å⁵

bond	literature values		our results	
	ρ	$\nabla^2\rho$	ρ	$\nabla^2\rho$
Si–Cl	hexacoordinate complex ^a		ClCl'	
	0.494	1.313	0.0183	0.0404
Si–Cl	pentacoordinate complex ^b		FCI'	
	0.549	1.891	0.017	0.0389
Si–F	0.740	17.41	0.0207	0.0525
Si–Cl	0.620	2.90	0.0214	0.0564

^aData taken from ref 12 (compound 1c). ^bData taken from ref 54 (compounds 2 and 3).

determines whether accumulation of charge at a given point (r) is stabilizing ($H(r) < 0$) or destabilizing ($H(r) > 0$). Thus, a value of ($H(r) < 0$) at BCP represents a significant covalent contribution and therefore a lowering of the potential energy associated with the concentration of charge between the nuclei^{61,62} (since, $h'/4m; \nabla^2\rho(r) = 2G(r) + V(r)$, while in the ionic interactions, the kinetic energy dominates at the BCPs resulting from a depletion of charge density in the interatomic surface or a contraction of charge density away from the BCP. The boundary conditions for the characterization of bond

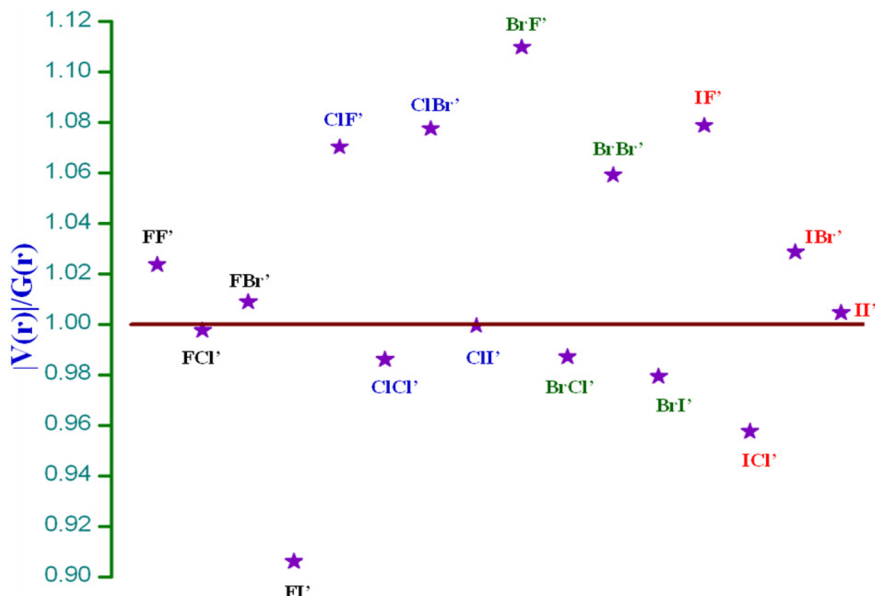


Figure 8. Plot of $|V(r)|/G(r)$ values at Si–X' BCPs of ISCs.

types^{63,64} have been presented in supporting figures (Supporting Information, Figure S4).

A positive Laplacian at the BCPs, a considerable $\rho(r)$ value, and a positive local energy density at the BCPs are indicative of a closed shell interaction (ionic), while those with negative local energy density $H(r)$ are transient interactions; in other words, these interactions are in between weakly covalent or weakly electrostatic regions.^{29,65} Therefore, FCl', FI', BrI', ClCl', BrCl', and ICl' are clear cases of closed shell interactions, while FF', FBr', ClF', ClBr', ClI', BrF', BrBr', BrCl', IF', IBr', and II' are of intermediate type.

Hence, QTAIM quantifies all the ISCs to be of ionic or transient type. However, a closer look at the more sensitive indicator of bonding nature, $|V(r)|/G(r)$ plot (Figure 8), shows that FI', which lies much below $|V(r)|/G(r) = 1$, is more ionic and that IF', BrF', and ClF', which are transient bonds, are more like shared interactions ($|V(r)|/G(r) = 2$).^{29,37} A contour plot of the electron density of BrF' cutting the plane above the center Si₆ ring, where the Lewis acid sites are located, is shown in Figure 7b. Figure 7c shows the Laplacian map of Si–X' where the apical Br' is found to have an intact core and a punctured or more diffusible valence shell, useful in hypercoordination.

From QTAIM analysis, it is clear that though the model of hypercoordinate bonding in these complexes are much weaker than those of the penta- and hexacoordinated Si complexes reported in the literature,⁶⁰ yet they exhibit both ionic and intermediate types of hypercoordinate bonds.

3.6. NBO Analysis. In NBO analysis, the input atomic orbital basis set is transformed via natural atomic orbitals (NAOs) and natural hybrid orbitals (NHOs) into natural bond orbitals (NBOs). The NBOs obtained correspond to the widely used Lewis picture in which two-centered bonds and lone pairs are localized. Such Lewis transformation of hypercoordinate bonds in ISCs would provide valuable information on the participation of orbitals and how the system can be understood on a chemical basis.^{35,66}

Natural population analysis computes the charge that is transferred between the donor and acceptor moieties and is an indicator of electrovalent bonding. The apical halides are found

to donate as much as 0.8el to a minimum of 0.1el to the Si, while the Si charges range from 1.28el to 0.07el apart from its tetracoordination (Table 5). The NPA charges of ISCs with X'

Table 5. NPA Charges Computed at B3LYP/6-311++g(d,p) for the ISCs

	NPA charges el						
	Si	X'	X	Si	X'	X	
FF'	1.28	-0.81	-0.67	BrF'	0.58	-0.75	-0.33
FCl'	1.24	-0.69	-0.67	BrCl'	0.52	-0.54	-0.34
FBr'	1.22	-0.60	-0.68	BrBr'	0.44	-0.40	-0.32
FI'	1.20	-0.55	-0.67	BrI'	0.32	-0.37	-0.26
ClF'	0.73	-0.76	-0.41	IF'	0.32	-0.74	-0.20
ClCl'	0.66	-0.58	-0.40	ICl'	0.21	-0.50	-0.19
ClBr'	0.62	-0.42	-0.41	IBr'	0.16	-0.38	-0.18
ClI'	0.60	-0.41	-0.40	II'	0.07	-0.10	-0.18

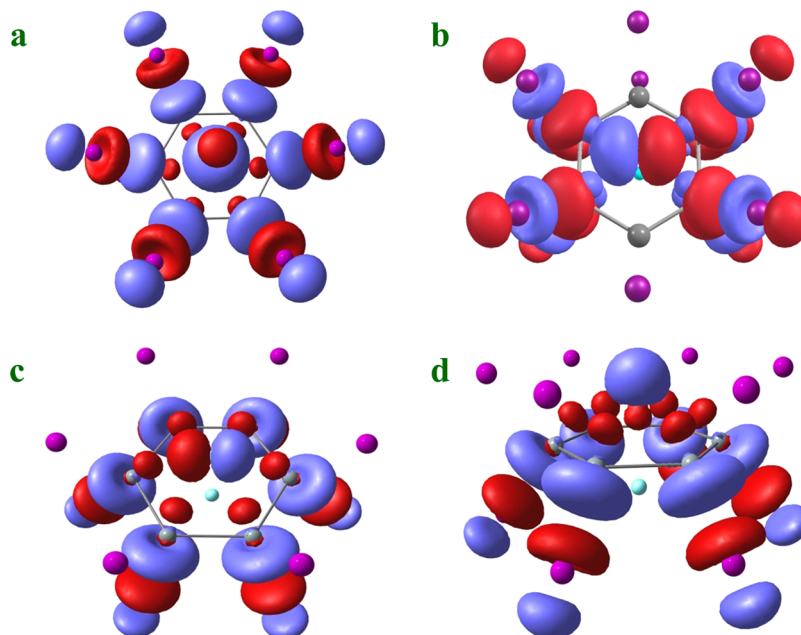
= I are less negative than the others as they are better donors. NPA charges of Si, X, and X' atoms are shown in Table 5. It is evident from the table that the order of electron donation among apical and ring halides varies with the electronegativity as follows I > Br > Cl > F, while the electron accepting capacity of Si depends on the electronegativity of the ring halides.

Wiberg and Mayor Bond orders of Si–X', Si–Si, and Si–X bonds are presented in Table 6. Mayer bond order was found to be larger than the Wiberg bond order, as in most of the compounds with higher differences in electronegativity.¹⁸ The Si–Si WBI, a measure of formal chemical bond order, varies from 0.80 to 0.86. This is higher than that in the corresponding perhalocyclohexasilanes (Supporting Information, Table S4). However, the Si–X' WBIs are <0.2 in all the complexes, which reveal their dominant ionic nature. The total WBI of Si atoms does not exceed 4 (3.01 to 3.93), which shows that the modified octet rule is not violated in these systems as expected in hypervalent compounds with electronegative ligands.⁴⁹

From second order perturbation energy analysis, it is found that the lone pair on the apical anion and the antibonding sigma orbitals of the Si–X bonds are the stabilizing interactions arising from the apical ions. Figure 9 depicts the natural bond

Table 6. Results of Wiberg and Mayer Bond Analysis at B3LYP/6-311++g(d,p)

	Wiberg bond analysis			WBI (total)	Mayer bond analysis		
	Si-X'	Si-Si	Si-X		Si	Si-X'	Si-Si
FF'	0.0575	0.8585	0.5144	3.0157	0.261	1.500	1.926
FCI'	0.0863	0.8524	0.5121	3.0677	0.198	1.411	1.944
FBr'	0.1120	0.8526	0.5035	3.1052	0.245	1.407	1.931
FI'	0.1180	0.8431	0.5033	3.1096	0.241	1.267	1.400
ClF'	0.0626	0.8447	0.8020	3.6094	0.296	1.536	1.894
ClCl'	0.1007	0.8364	0.8020	3.6857	0.272	1.455	1.923
ClBr'	0.1348	0.8382	0.7856	3.7293	0.320	1.444	1.895
ClI'	0.1303	0.8357	0.7933	3.7388	0.285	1.202	1.719
BrF'	0.0637	0.8353	0.8495	3.7049	0.289	1.516	1.877
BrCl'	0.1047	0.8512	0.8445	3.8246	0.265	1.459	1.935
BrBr'	0.1302	0.8299	0.8404	3.8328	0.309	1.440	1.901
BrI'	0.1425	0.8180	0.8130	3.7928	0.253	1.184	1.742
IF'	0.0621	0.8289	0.9086	3.8247	0.167	1.234	1.840
ICl'	0.1023	0.8084	0.8855	3.8382	0.217	1.206	1.766
IBr'	0.1213	0.8148	0.8927	3.9091	0.237	1.215	1.822
I'	0.1633	0.8120	0.8685	3.9567	0.270	1.199	1.800

Figure 9. Ground state stabilizing NBOs in I'' showing $n_{X'} \rightarrow \sigma^*_{(Si-X)}$ interactions.

orbitals responsible for the $n_{X'(\text{LP}4)} \rightarrow \sigma^*_{(Si-X)}$ of I''. Of the four lone pairs available on the X' atoms, LP(4) involved in the favorable interaction with Si-X $\sigma^*_{(Si-X)}$ is predominantly of sp character and has low occupancies (see Supporting Information, Table S5) and is depicted in Figure 9d. LP(2) and LP(3) are of p and sp character, respectively (Figure 9b,c). Hence, it is understood that these $n_{X'} \rightarrow \sigma^*_{(Si-X)}$ are the interactions that stabilize the system. It is also interesting to note that the Si-X $\sigma^*_{(Si-X)}$ and every Si-Si bonding orbital have the strongest interaction energies, stabilizing the planar structures.

4. CONCLUSIONS

Si-X' bonds in inverse sandwich complexes where 2:6 anions/Si interactions exist are examined and the following results are summarized: Hypercoordination in these complexes are much weaker than the perfect hexa- and pentacoordinate Si systems hitherto known. The anion ring interaction seems to be more

of a donor–acceptor type. While the driving force for hypercoordination is the lewis acid site present above and below the Si₆ core, the apical ions participate in a very weak covalent interaction or a mere ionic bonding in most cases as identified by QTAIM. Size and acidity of the Lewis sites and the polarizability of the binding anions dictate the extent of donation of electrons to Si. Ring halides play a decisive role by depleting the electron densities at Si atom. ISCs with strong Lewis acid sites and poorly polarizing donor halides are found to have lesser percent covalency of interaction. The apical ion coordination was found to be stabilized by $n_{(X')} \rightarrow \sigma^*_{(Si-X)}$. BrF', ClBr', and IF', which are lying closer toward shared interactions, may be useful as nanoscale building blocks. The study reveals that these weak hypercoordinate Si systems possess sites very amenable for tuning and will be candid in the design of more such novel entities with prospective applications in Si nanostructures.

■ ASSOCIATED CONTENT

§ Supporting Information

Calculated results of energy decomposition analysis, van der Waals radii analysis, ELF maps, SFO analysis, and AIM analysis along with coordinates of ISCs. This material is available free of charge via the Internet at <http://pubs.acs.org>.

■ AUTHOR INFORMATION

Corresponding Author

*(P.V.) Fax: +91 431 2407045. E-mail: venuvanalingam@yahoo.com. Homepage: http://www.bdu.ac.in/schools/chemistry/chemistry/dr_p_venuvanalingam.php.

Notes

The authors declare no competing financial interest.

■ ACKNOWLEDGMENTS

S.AV. thanks the University Grants Commission (UGC), India, and Bishop Heber College, Tiruchirappalli, for FDP program (ref no. F.ETFTNBD030/FIP-XI PLAN). R.V.S. thanks the University Grants Commission, India, for Senior Research Fellowship through the Maulana Azad National Fellowship (ref no. F.40-17(C/M)/2009(SA-III/MANF)).

■ REFERENCES

- (1) Doronina, E. P.; Belogolova, E. F.; Sidorkin, V. F. Molecular Design of Hypercoordinated Silacyclophanes. *Organometallics* **2011**, *30*, 5595–5603.
- (2) Koukaras, E.; Zdetsis, A. Multidecker Sandwiches of Silicon–Carbon Clusters. *Organometallics* **2009**, *28*, 4308–4315.
- (3) Gerlach, D.; Brendler, E.; Heine, T.; Wagler, J. Dianion of Pyrrole-2-N-(*o*-hydroxyphenyl)carbaldimine As an Interesting Tridentate (ONN) Ligand System in Hypercoordinate Silicon Complexes. *Organometallics* **2007**, *26*, 234–240.
- (4) Kost, D.; Kalikhman, I. Hypercoordinate Silicon Complexes Based on Hydrazide Ligands. A Remarkably Flexible Molecular System. *Acc. Chem. Res.* **2008**, *42*, 303–314.
- (5) Parameswaran, P.; Frenking, G. Chemical Bonding in Transition Metal Complexes with Beryllium Ligands $[(\text{PMe}_3)_2\text{M}-\text{BeCl}_2]$, $[(\text{PMe}_3)_2\text{M}-\text{BeClMe}]$, and $[(\text{PMe}_3)_2\text{M}-\text{BeMe}_2]$ ($\text{M}=\text{Ni}, \text{Pd}, \text{Pt}$). *J. Phys. Chem. A* **2009**, *114*, 8529–8535.
- (6) Perez-Peralta, N.; Boldyrev, A. I. Ab Initio Study of Lithiathion of the Si4-Cluster. *J. Phys. Chem. A* **2011**, *115*, 11551–11558.
- (7) Tiznado, W.; Perez-Peralta, N.; Islas, R.; Toro-Labbe, A.; Ugalde, J. M.; Merino, G. Designing 3-D Molecular Stars. *J. Am. Chem. Soc.* **2009**, *131*, 9426–9431.
- (8) Wagler, J.; Gerlach, D.; Roewer, G. 8-Oxyquinolate and 8-Oxyquinaldinate in Silicon Complex Chemistry: A New Face of Old Ligands. *Chem. Heterocycl. Compd.* **2006**, *42*, 1557–1567.
- (9) Zubarev, D. Y.; Alexandrova, A. N.; Boldyrev, A. I.; Cui, L. F.; Li, X.; Wang, L. S. On the Structure and Chemical Bonding of $\text{Si}_6^{(2)}$ and $\text{Si}_6^{(2)}$ in $\text{NaSi}_6^{(2)}$ upon Na^+ Coordination. *J. Chem. Phys.* **2006**, *124*, 124305.
- (10) Jensen, W. B. The Origin of the Term "Hypervalent". *J. Chem. Educ.* **2006**, *83*, 1751.
- (11) Yang, Y. Hexacoordinate Bonding and Aromaticity in Silicon Phthalocyanine. *J. Phys. Chem. A* **2010**, *114*, 13257–13267.
- (12) Fester, G. W.; Wagler, J.; Brendler, E.; Böhme, U.; Gerlach, D.; Kroke, E. Octahedral HSiCl_3 and HSiCl_2Me Adducts with Pyridines. *J. Am. Chem. Soc.* **2009**, *131*, 6855–6864.
- (13) Kobayashi, J.; Ishida, K.; Kawashima, T. Synthesis of a Heptacoordinate Trichlorosilane with a Tetradentate Ligand and Unusual Stability for Nucleophilic Substitution. *Silicon Chem.* **2002**, *1*, 351–354.
- (14) Okazaki, T.; Galembeck, S. E.; Kenneth, K. Novel Examples of Three-Dimensional Aromaticity: 1,3-Dehydro-silaadamantane Dications. A Theoretical (DFT, GIAO NMR, NICS) Study. *J. Org. Chem.* **2002**, *67*, 8721–8725.
- (15) Brook, A. G. Molecular Rearrangements of Organosilicon Compounds. *Acc. Chem. Res.* **1974**, *7*, 77–84.
- (16) Boyraz, O.; Jalali, B. Demonstration of a Silicon Raman Laser. *Opt. Express* **2004**, *12*, 5269–5273.
- (17) Pavesi, L.; Lockwood, D. J. *Silicon photonics*; Springer Verlag: Berlin, Germany, 2004; Vol. 1.
- (18) Kim, B. K.; Choi, S. B.; Kloos, S. D.; Boudjouk, P. Synthesis and Characterization of New Cationic Hexacoordinate Silanes. *Inorg. Chem.* **2000**, *39*, 728–731.
- (19) Dai, X.; Anderson, K. J.; Schulz, D. L.; Boudjouk, P. Coordination Chemistry of $\text{Si}_5\text{Cl}_{10}$ with Organocyanides. *Dalton Trans.* **2010**, *39*, 11188–11192.
- (20) Vach, H. Electron-Deficiency Aromaticity in Silicon Nano-clusters. *J. Chem. Theory Comput.* **2012**, *8*, 2088–2094.
- (21) Vach, H. Ultrastable Silicon Nanocrystals Due to Electron Delocalization. *Nano lett.* **2011**, *11*, 5477–5481.
- (22) Dai, X.; Schulz, D. L.; Braun, C. W.; Ugrinov, A.; Boudjouk, P. Inverse Sandwich Complexes of Perhalogenated Cyclohexasilane. *Organometallics* **2010**, *29*, 2203–2205.
- (23) Dai, X.; Choi, S. B.; Braun, C. W.; Vaidya, P.; Kilina, S.; Ugrinov, A.; Schulz, D. L.; Boudjouk, P. Halide Coordination of Perhalocyclohexasilane Si_6X_{12} ($\text{X}=\text{Cl}$ or Br). *Inorg. Chem.* **2011**, *50*, 4047.
- (24) Bader, R. F. W. Atoms in Molecules. *Acc. Chem. Res.* **1985**, *18*, 9–15.
- (25) Pokhodnya, K.; Olson, C.; Dai, X.; Schulz, D. L.; Boudjouk, P.; Sergeeva, A. P.; Boldyrev, A. I. Flattening a Puckered Cyclohexasilane Ring by Suppression of the Pseudo-Jahn–Teller Effect. *J. Chem. Phys.* **2011**, *134*, 014105.
- (26) Gostevskii, B.; Zamstein, N.; Korlyukov, A. A.; Baukov, Y. I.; Botoshansky, M.; Kaftory, M.; Kocher, N.; Stalke, D.; Kalikhman, I.; Kost, D. Donor-Stabilized Silyl Cations. 11. Bis-Zwitterionic Penta-and Hexacoordinate Silicon Dicarboxylate Complexes Derived from $(\text{ClCH}_2)_2\text{SiCl}_2$ through Double Internal Displacement of Chloride. *Organometallics* **2006**, *25*, 5416–5423.
- (27) Li, S. D.; Guo, J. C.; Miao, C. Q.; Ren, G. M. C_{2h} ($\text{B}_n\text{E}_m\text{Si})_2\text{H}_2$ Molecules ($\text{E}=\text{B}, \text{C}, \text{Si}; n=3–6; m=1, 2$) Containing Double Planar Tetra-, Penta-, and Hexacoordinate Silicons. *J. Phys. Chem. A* **2005**, *109*, 4133–4136.
- (28) Islas, R.; Heine, T.; Ito, K.; Schleyer, P. v. R.; Merino, G. Boron Rings Enclosing Planar Hypercoordinate Group 14 Elements. *J. Am. Chem. Soc.* **2007**, *129*, 14767–14774.
- (29) Sidorkin, V. F.; Belogolova, E. F.; Pestunovich, V. A. Molecular Design of Neutral Intramolecular Complexes Bearing Two Silicon Atoms Anchored by a Carbonyl Oxygen Atom: $\text{N}_2\text{N}'\text{-Bis(silylmethyl)}$ -Propylene Ureas. *Chem.—Eur. J.* **2006**, *12*, 2021–2031.
- (30) Zdetsis, A. D. The Boron Connection: A Parallel Description of Aromatic, Bonding, and Structural Characteristics of Hydrogenated Silicon–Carbon Clusters and Isovalent Carboranes. *Inorg. Chem.* **2008**, *47*, 8823–8829.
- (31) Zdetsis, A. D. Bonding and Structural Characteristics of Zn , Cu , and Ni -Encapsulated Si Clusters: Density-Functional Theory Calculations. *Phys. Rev. B* **2007**, *75*, 085409.
- (32) Perdew, J. P. Density-Functional Approximation for the Correlation Energy of the Inhomogeneous Electron Gas. *Phys. Rev. B* **1986**, *33*, 8822.
- (33) Häussermann, U.; Dolg, M.; Stoll, H.; Preuss, H.; Schwerdtfeger, P.; Pitzer, R. Accuracy of Energy-Adjusted Quasirelativistic ab Initio Pseudopotentials. *Mol. Phys.* **1993**, *78*, 1211–1224.
- (34) Frisch, M. J.; Trucks, G. W.; Schlegel, H. B.; Scuseria, G. E.; Robb, M. A.; Cheeseman, J. R.; Scalmani, G.; Barone, V.; Mennucci, B.; Petersson, G. A.; Nakatsuji, H.; Caricato, M.; Li, X.; Hratchian, H. P.; Izmaylov, A. F.; Bloino, J.; Zheng, G.; Sonnenberg, J. L.; Hada, M.; Ehara, M.; Toyota, K.; Fukuda, R.; Hasegawa, J.; Ishida, M.; Nakajima, T.; Honda, Y.; Kitao, O.; Nakai, H.; Vreven, T.; Montgomery, J. A., Jr.; Peralta, J. E.; Ogliaro, F.; Bearpark, M.; Heyd, J. J.; Brothers, E.; Kudin, K. N.; Staroverov, V. N.; Kobayashi, R.; Normand, J.; Raghavachari, K.; Rendell, A.; Burant, J. C.; Iyengar, S. S.; Tomasi, J.; Cossi, M.; Rega,

- N.; Millam, J. M.; Klene, M.; Knox, J. E.; Cross, J. B.; Bakken, V.; Adamo, C.; Jaramillo, J.; Gomperts, R.; Stratmann, R. E.; Yazeyev, O.; Austin, A. J.; Cammi, R.; Pomelli, C.; Ochterski, J. W.; Martin, R. L.; Morokuma, K.; Zakrzewski, V. G.; Voth, G. A.; Salvador, P.; Dannenberg, J. J.; Dapprich, S.; Daniels, A. D.; Farkas, O.; Foresman, J. B.; Ortiz, J. V.; Cioslowski, J.; Fox, D. J. *Gaussian 09*, revision B.01; Gaussian, Inc.: Wallingford, CT, 2009.
- (35) Reed, A. E.; Curtiss, L. A.; Weinhold, F. Intermolecular Interactions from a Natural Bond Orbital, Donor–Acceptor Viewpoint. *Chem. Rev.* **1988**, *88*, 899–926.
- (36) Perdew, J. P. Density-Functional Approximation for the Correlation Energy of the Inhomogeneous Electron Gas. *Phys. Rev. B* **1986**, *33*, 8822–8824.
- (37) Te Velde, G.; Bickelhaupt, F. M.; Baerends, E. J.; Fonseca Guerra, C.; van Gisbergen, S. J. A.; Snijders, J. G.; Ziegler, T. Chemistry with ADF. *J. Comput. Chem.* **2001**, *22*, 931–967.
- (38) Wagner, F. R.; Bezugly, V.; Kohout, M.; Grin, Y. Charge Decomposition Analysis of the Electron Localizability Indicator: A Bridge between the Orbital and Direct Space Representation of the Chemical Bond. *Chem.—Eur. J.* **2007**, *13*, 5724–5741.
- (39) Milov, A. A.; Minyaev, R. M.; Minkin, V. I. Intramolecular Hypervalent Interaction in the Conjugate Five-Membered Rings. *J. Phys. Chem. A* **2011**, *115*, 12973–12982.
- (40) Jacobsen, H. Hypovalency: A Kinetic-Energy Density Description of a 4c–2e Bond. *Dalton Trans.* **2009**, 4252–4258.
- (41) Sajith, P.; Suresh, C. H. Quantification of the Trans Influence in Hypervalent Iodine Complexes. *Inorg. Chem.* **2012**, *51*, 967–977.
- (42) Poulsen, D. A.; Werstiuk, N. H. A QTAIM and Electron Delocalization Computational Study of *tert*-Butylmethylene, Trimethylsilylmethylene, and Trimethylgermylmethylene. A New Method for Unambiguously Characterizing the Bonding between Pairs of Atoms in Reaction Intermediates. *J. Chem. Theory Comput.* **2006**, *2*, 75–80.
- (43) Juarez-Perez, E. J.; Aragoni, M. C.; Arca, M.; Blake, A. J.; Devillanova, F. A.; Garau, A.; Isai, F.; Lippolis, V.; Nunez, R.; Pintus, A.; Wilson, C. A Unique Case of Oxidative Addition of Interhalogens IX (X = Cl, Br) to Organosilene Ligands: Nature of the Chemical Bonding in Asymmetric I-Se-X Polarised Hypervalent Systems. *Chem.—Eur. J.* **2011**, *17*, 11497–11514.
- (44) Lu, T.; Chen, F. Multiwfns: A Multifunctional Wavefunction Analyzer. *J. Comput. Chem.* **2012**, *33*, 580–592.
- (45) Biegler-König, F.; Schönbohm, J.; Bayles, D. AIM2000: A Program to Analyze and Visualize Atoms in Molecules. *J. Comput. Chem.* **2001**, *22*, 545.
- (46) Bondi, A. van der Waals Volumes and Radii. *J. Phys. Chem.* **1964**, *68*, 441–451.
- (47) Cordero, B.; Gómez, V.; Platero-Prats, A. E.; Revés, M.; Echeverría, J.; Cremades, E.; Barragán, F.; Alvarez, S. Covalent Radii Revisited. *Dalton. Trans.* **2008**, 2832–2838.
- (48) Dai, X.; Choi, S. B.; Braun, C. W.; Vaidya, P.; Kilina, S.; Ugrinov, A.; Schulz, D. L.; Boudjouk, P. Halide Coordination of Perhalocyclohexasilane Si_6X_{12} (X = Cl or Br). *Inorg. Chem.* **2011**, *50*, 4047–4053.
- (49) Noury, S.; Silvi, B.; Gillespie, R. J. Chemical Bonding in Hypervalent Molecules: Is the Octet Rule Relevant? *Inorg. Chem.* **2002**, *41*, 2164–2172.
- (50) Contreras-García, J.; Johnson, E. R.; Keinan, S.; Chaudret, R.; Piquemal, J. P.; Beratan, D. N.; Yang, W. NCIPILOT: A Program for Plotting Non-Covalent Interaction Regions. *J. Chem. Theory Comput.* **2011**, *7*, 625.
- (51) Savin, A.; Nesper, R.; Wengert, S.; Fässler, T. F. ELF: The Electron Localization Function. *Angew. Chem., Int. Ed.* **2003**, *36*, 1808–1832.
- (52) Yang, Y. Two-Center Two-Electron Covalent Bonds with Deficient Bonding Densities. *J. Phys. Chem. A* **2012**, *116*, 10150–10159.
- (53) Xinying, L. Interaction between Coinage Metal Cations M (II) and Xe: CCSD (T) Study of MXe_n^{2+} (M= Cu, Ag, and Au, n= 1–6). *J. Chem. Phys.* **2012**, *137*, 124301–124301–124307.
- (54) McGrady, G. S.; Sirsch, P.; Chatterton, N. P.; Ostermann, A.; Gatti, C.; Altmannshofer, S.; Herz, V.; Eickerling, G.; Scherer, W. Nature of the Bonding in Metal–Silane σ -Complexes. *Inorg. Chem.* **2009**, *48*, 1588–1598.
- (55) Popelier, P.; Aicken, F.; O'Brien, S. Atoms in Molecules. In *Chemical Modelling: Applications and Theory*; The Royal Society of Chemistry: Cambridge, U.K., **2000**; Vol. 1, pp 143–198.
- (56) Pendás, A. M.; Francisco, E.; Blanco, M. A.; Gatti, C. Bond Paths As Privileged Exchange Channels. *Chem.—Eur. J.* **2007**, *13*, 9362–9371.
- (57) Ponec, R.; Gatti, C. Do the Structural Changes Defined by the Electron Density Topology Necessarily Affect the Picture of the Bonding? *Inorg. Chem.* **2009**, *48*, 11024–11031.
- (58) Pachos, L. F. A Theoretical Study of the Intramolecular Interaction between Proximal Atoms in Planar Conformations of Biphenyl and Related Systems. *Struct. Chem.* **2007**, *18*, 785–795.
- (59) Sidorkin, V. F.; Belogolova, E. F.; Pestunovich, V. A. Molecular Design of Bis-Chelate N-Donor-Stabilized Silaethenes: Theoretical Study of 1,1-Bis[N-(dimethylamino)acetimidato] Silene. *Organometallics* **2004**, *23*, 2389–2396.
- (60) Kocher, N.; Henn, J.; Gostevskii, B.; Kost, D.; Kalikhman, I.; Engels, B.; Stalke, D. Si–E (E = N, O, F) Bonding in a Hexacoordinated Silicon Complex: New Facts from Experimental and Theoretical Charge Density Studies. *J. Am. Chem. Soc.* **2004**, *126*, 5563–5568.
- (61) Mohajeri, A.; Alipour, M.; Mousaei, M. Halogen–Hydride Interaction between Z–X (Z = CN, NC; X = F, Cl, Br) and H–Mg–Y (Y = H, F, Cl, Br, CH_3). *J. Phys. Chem. A* **2011**, *115*, 4457–4466.
- (62) Woodford, J. N. Density Functional Theory and Atoms-in-Molecules Investigation of Intramolecular Hydrogen Bonding in Derivatives of Malonaldehyde and Implications for Resonance-Assisted Hydrogen Bonding. *J. Phys. Chem. A* **2007**, *111*, 8519–8530.
- (63) Cremer, D.; Kraka, E. Chemical Bonds without Bonding Electron Density: Does the Difference Electron-Density Analysis Suffice for a Description of the Chemical Bond? *Angew. Chem., Int. Ed.* **2003**, *42*, 627–628.
- (64) Cremer, D.; Kraka, E. A Description of the Chemical Bond in Terms of Local Properties of Electron Density and Energy. *Croat. Chem. Acta* **1984**, *57*, 1259–1281.
- (65) Ottosson, C. H.; Cremer, D. Intramolecularly Stabilized Phenylsilyl and Anthrylsilyl Cations. *Organometallics* **1996**, *15*, 5309–5320.
- (66) Glendening, E.; Reed, A.; Carpenter, J.; Weinhold, F. NBO, version 3.1; University of Wisconsin—Madison: Madison, WI, 1988.